Elastic Constants and Anisotropy of $MgSiO_3$ Perovskite, Periclase, and SiO_2 at High Pressure

Lars Stixrude

Dept. of Geological Sciences, University of Michigan, Ann Arbor

We review recent results of first principles theory as applied to the elastic constants of important deep earth phases at high pressure, including $MgSiO_3$ perovskite, MgO periclase and the stishovite, $CaCl_2$ and columbite phases of SiO_2. The foundation and implementation of the theoretical technique, the plane-wave pseudopotential method, is briefly discussed as is the method for determining the structure and elastic constants at high pressure. The results show that predicted elastic constants are in good agreement with experiment: RMS deviation are 5 %, 7 % and 4 %, respectively for perovskite, periclase and stishovite. Much of the difference can be accounted for by the difference in temperature between the athermal calculations and the 300 K experiments. We discuss these results in terms of seismological observations paying particular attention to 1) the properties of aggregates and 2) anisotropy. Comparison of the seismic wave velocities of isotropic mono-phase aggregates with those of the lower mantle show that the P- and S-wave velocities of perovskite are consistent with those of the deep earth, supporting the view that this mineral is the most abundant constituent of the lower mantle. The properties of anisotropic mono-phase aggregates are estimated based on the theoretical results for single crystals and simple models of flow in D″ and of mineralogical deformation mechanisms. We find that the SH/SV anisotropy is large for aggregates of perovskite, periclase and silica (6-8 % in magnitude) compared with that observed in D″. While mono-phase aggregates of silica exhibit fast SH velocity at pressures corresponding to D″, perovskite and periclase have slow SH velocities. We discuss the implications of these results for the origin of anisotropy in D″.

1. INTRODUCTION

The elasticity of minerals determines the solid earth's response to a wide variety of loads that have time scales shorter than the Maxwell relaxation time and magnitudes less than the shear strength. Elasticity controls such diverse geologic phenomena as the form of sedimentary basins, moats and peripheral bulges surrounding oceanic volcanos, and forearc bulges. In the deep earth where the Maxwell relaxation time is much shorter than that in the lithosphere, elasticity is most important for understanding the propagation of seismic energy.

Seismological observations of the earth's interior in principle contain a wealth of information concerning its composition, thermal state, and dynamics. This information has proven difficult to extract, primarily because the elastic constants of mantle minerals under the relevant conditions are essentially unknown. While the elastic constants of most major mantle phases are known at ambient conditions, and, in some cases at ambient pressure and high temperature [*Bass*, 1995; *Anderson and Isaak*, 1995], little is known of the elastic

The Core-Mantle Boundary Region
Geodynamics 28

constants of any material at mantle pressures. This is a serious limitation as pressure is expected to have a much greater effect on elastic properties over the range of pressure and temperature relevant to the deep mantle.

Our lack of knowledge of high pressure elasticity has meant that we have been unable to make use of those aspects of mantle elasticity that are unique to the solid state: anisotropy, and the propagation of shear waves. This limitation likely accounts for the lack of consensus concerning the composition of the lower mantle [*Jeanloz and Knittle*, 1989; *Bukowinski and Wolf*, 1990; *Stixrude et al.*, 1992; *Wang et al.*, 1994; *Bina and Silver*, 1997] - of seismologically observable properties, it is precisely those of which we are ignorant (the shear modulus) which are most sensitive to composition, temperature and phase.

Recent experimental advances have led to the first measurements of the elastic constants of mantle minerals at the relevant pressures [*Zaug et al.*, 1993; *Duffy et al.*, 1995; *Chen et al.*, 1996]. A variety of techniques including light-scattering and ultrasonic methods hold tremendous promise for revealing the elasticity of mantle minerals at mantle pressure and temperature conditions. These methods have not yet been applied to the major minerals of the lower mantle.

Major advances in theory and computation now make it possible to calculate the full elastic constant tensor of mantle minerals from first principles [*Karki et al.*, 1997a; *Karki et al.*, 1997b; *Karki et al.*, 1997c; *da Silva et al.*, 1997]. These methods are parameter-free and are completely independent of experiment. They thus provide the ideal complement to the experimental approach, allowing for important cross-checks between laboratory observation and theory. First principles methods are unlimited in the range of pressure that they can explore and are equally applicable in principle to all mantle materials. They represent a potentially important tool for studying the wide range of pressure and composition encountered in the earth's interior.

We briefly discuss theoretical methods below, including techniques for calculating the full elastic constant tensor. We review some recent results on the most abundant constituents of the lower mantle [*Karki et al.*, 1997a; *Karki et al.*, 1997b; *Karki et al.*, 1997d; *Karki et al.*, 1997c]. Theory is compared with seismological observation with particular emphasis on the one-dimensional isotropic structure of the lower mantle, and observations of anisotropy in the deepest portions of this region. Careful attention is paid to the anisotropy of single crystals versus that of aggregates, and possible texturing mechanisms in the earth's interior.

2. THEORY

2.1. Density Functional Theory

The calculations are based on density functional theory [*Hohenberg and Kohn*, 1964; *Kohn and Sham*, 1965], in principle an exact theory of the ground state electronic total energy and band structure. We discuss the two essential approximations that are made in our calculations, 1) the local density approximation and in the following subsection, 2) the pseudopotential approximation. The methods for determining the structure and elastic constants are briefly described in the last subsection.

The essence of this theory is the proof that the ground state electronic properties of a material are a unique functional of the charge density $\rho(\vec{r})$. This central feature is appealing because the charge density is experimentally observable, for example, by x-ray diffraction. A variational principle leads to a set of single-particle, Schrödinger-like Kohn-Sham equations, with an effective potential

$$V_{KS} = V_{e-n}\left[\rho(\vec{r})\right] + V_{e-e}\left[\rho(\vec{r})\right] + V_{xc}\left[\rho(\vec{r})\right] \qquad (1)$$

where the first two terms are the Coulomb potentials due to the nuclei and the other electrons, and the last, the exchange-correlation potential, subsumes the complex many-body interactions among the electrons. The power of density functional theory is that it allows one to calculate, in principle, the exact many-body total energy of a system from a set of single-particle equations. In practice, exact solutions are impossible at present because the exact form of V_{xc} is currently unknown.

Simple approximations to the exchange-correlation functional have proven to be very successful in studies of silicates and essentially all other classes of solids. In this study, we use the most widely studied approximation, the Local Density Approximation (LDA), which replaces V_{xc} at every point in the crystal by the precisely known value for a free electron gas with a density equal to the local charge density [*Lundqvist and March*, 1987]. The success of the LDA can be understood at a fundamental level in terms of the satisfaction of exact sum rules for the exchange-correlation hole [*Gunnarsson and Lundqvist*, 1976].

LDA calculations of silicates and oxides of geophysical interest agree very well with experimental data. The error due to the LDA approximation can be evaluated by comparing Linearized Augmented Plane Wave (LAPW) calculations, which make no further essential approximations beyond the LDA, with experiment. It

has been found that errors in volumes are typically 1-4 % with theoretical volumes being uniformly smaller than experimental [*Mehl et al.*, 1988; *Cohen*, 1991; *Cohen*, 1992; *Stixrude and Cohen*, 1993]. Part of this small difference is due to the higher temperatures of experiments (300 K) compared with the athermal calculations [*Mehl et al.*, 1988]. This is a highly satisfactory level of agreement for a theory which is parameter free and independent of experiment.

2.2. The Pseudopotential Method

The basis of this method is the simple observation that only the valence electrons participate in the response of the crystal to most perturbations. Unless the perturbation is of very high energy (comparable to the binding energy of the core states), the tightly bound core states remain essentially unchanged. It is reasonable then to assume for most applications that the core electrons are frozen. The frozen core approximation is satisfied to a high degree of accuracy for many applications, for example in the case of finite strains of magnitudes typically encountered in the earth's interior.

The pseudopotential method replaces the nucleus and core electrons with a single object, the pseudopotential, which has the same scattering properties [*Pickett*, 1989]. The advantages of the pseudopotential method are 1) spatial variations in the pseudopotential are much less rapid than the bare Coulomb potential of the nucleus and 2) one need solve only for the valence electrons which show much less rapid spatial variation than the core electrons. This means that in the solution of the Kohn-Sham equations, potential and charge density can be represented by a particularly simple, complete and orthogonal set of basis functions (plane-waves) of manageable size (typically $10^3 - 10^5$ basis functions are required). With this basis set, evaluation of total energies, stresses, and forces acting on the atoms is particularly efficient.

The increased computational efficiency of the pseudopotential method comes at the cost of additional assumptions; the frozen core approximation, already mentioned, and, more seriously, the pseudopotential itself, which is an approximation to the potential that the valence electrons "see". The construction of the pseudopotential is a non-unique process, and several different methods have been developed [*Vanderbilt*, 1990; *Troullier and Martins*, 1991; *Kresse et al.*, 1992]. Care must be taken to demonstrate the transferability of the pseudopotentials generated by a particular method and to compare with all electron calculations where these are available. When these conditions are met, the error due to the pseudopotential is generally small (few percent in volume for earth materials) [*Kiefer et al.*, 1997].

In this study, pseudopotentials are generated by the Q_c-tuning method [*Lin et al.*, 1993], which yield results in excellent agreement with LAPW calculations where these are available [*Karki et al.*, 1997a; *Karki et al.*, 1997d; *Karki et al.*, 1997c], and with calculations [*Wentzcovitch et al.*, 1995] based on other pseudopotentials [*Troullier and Martins*, 1991]. Computational parameters were chosen so that calculated stresses were converged to within 0.02 GPa: the number of plane waves per atom ranges from 2,400 (MgO) to 22,000 ($MgSiO_3$) (maximum kinetic energy 62-66 Ry); the Brillouin zone is sampled on a 4x4x4 (oxides) or 4x4x2 ($MgSiO_3$) Monkhurst-Pack [*Monkhurst and Pack*, 1976] special k-point mesh.

2.3. Structural Optimization and Determination of Elastic Constants

Only recently has it become possible to determine from first principles the ground state atomic arrangement in a relatively complex structure such as $MgSiO_3$ perovskite [*Wentzcovitch et al.*, 1993]. The key innovation has been the development of a structural optimization strategy based on a pseudo-Lagrangian that treats the components of the strain tensor and the atomic positions as dynamical variables [*Wentzcovitch*, 1991]. The optimization is performed at constant pressure. At each step of the dynamical trajectory, the Hellman-Feynman forces and stresses [*Nielsen and Martin*, 1985] acting, respectively, on the nuclei and lattice parameters are evaluated and used to generate the next configuration. The optimization is complete when the forces on the nuclei vanish and the stress is hydrostatic and balances the applied pressure. This is an efficient procedure, requiring on the order of 10-20 steps even for a relatively complex structure such as orthorhombic perovskite with three lattice parameters and 7 internal degrees of freedom [*Wentzcovitch et al.*, 1995]. Even larger and more complex structures have been studied with this technique (e.g. olivine) [*Wentzcovitch and Stixrude*, 1997].

Once the equilibrium structure at a given pressure is determined, one can calculate the elastic constants. This is done in a straightforward way by applying a deviatoric strain to the lattice and calculating the resulting stress tensor. The elastic constant, c_{ijkl} is then given by the ratio of stress, σ_{ij} to strain ϵ_{ij}

$$\sigma_{ij} = c_{ijkl}\epsilon_{kl} \qquad (2)$$

To ensure that the calculated elastic constants refer to the appropriate linear (infinitesimal strain) regime, the ratio of stress to strain is calculated for several values of the strain magnitude (1-4 %) and then extrapolated to the limit of zero strain. Care must be taken to re-optimize the positions of the atoms in each strained configuration since vibrational modes typically couple with lattice strains in silicate structures.

2.4. Derived Quantities: Single Crystal Elastic Wave Velocities

Once the full elastic constant tensor has been determined, it is straightforward to calculate the elastic wave velocities of the single crystal for arbitrary propagation direction, $\vec{n}$ from the Cristoffel equation. The eigenvalues and eigenvectors of the matrix

$$c_{ijkl}n_j n_l \tag{3}$$

yield the moduli (ρV^2) and polarizations, respectively of the three elastic waves, where ρ is the density and V is the speed of the wave. The three eigensolutions correspond to a quasi-longitudinal or P wave (velocity V_P) and two quasi-shear waves (velocities V_{S1} and V_{S2}). Examination of the eigenvectors shows that unless the anisotropy is very large (greater than 20 %), the modes are nearly pure (P-waves more than 90 % pure). Only in the vicinity of the stishovite to $CaCl_2$ phase transition have we found P-S mode mixing exceeding 10 %.

We summarize the dependence of elastic wave velocities on propagation direction in the single crystal by three measures of the anisotropy:

$$\Delta_{P,azimuthal} = \frac{max[V_P(\vec{n})] - min[V_P(\vec{n})]}{V_{Pagg}} \tag{4}$$

$$\Delta_{S,azimuthal} = \frac{max[V_S(\vec{n})] - min[V_S(\vec{n})]}{V_{Sagg}} \tag{5}$$

$$\Delta_{S,polarization} = \frac{max|V_{S1}(\vec{n}) - V_{S2}(\vec{n})|}{V_{Sagg}} \tag{6}$$

which are, respectively, the maximum single-crystal azimuthal anisotropy in P- and S-waves and the maximum single-crystal polarization anisotropy of S-waves. The quantities V_{Pagg} and V_{Sagg} are the isotropic aggregates velocities.

3. PROPERTIES OF AGGREGATES

The earth's interior is a multi-phase aggregate, and any comparison of the properties of minerals with seismology must take this into account. For the case of geophysical interest, where the seismic wavelength is much larger than the size of the component crystals, the elastic wave velocities of an aggregate can be uniquely calculated from the single crystal elastic constants once the texture, that is the positions, shapes, and orientations of the constituent grains are known.

Because we have little knowledge of the texture of the deep mantle, we consider geophysically motivated approximations to the texture of aggregates in the earth's interior, for which the estimation of elastic wave velocities is relatively straightforward. The simplest case is the isotropic mono-phase aggregate, in which crystals of a single phase are oriented randomly. It is worth remembering that even for this simple case, the aggregate velocities are inherently uncertain since the shapes of the grains have not been specified [*Watt et al.*, 1976]. However, it is possible to place strict bounds on the aggregate velocities, which, in most cases, differ by a few percent or less. Here, we have estimated the velocities of isotropic mono-phase aggregates by the average of the Hashin-Shtrikman bounds [*Hashin and Shtrikman*, 1962; *Meister and Peselnick*, 1966] in the case of cubic and tetragonal crystals, and by the Voigt-Reuss-Hill average [*Hill*, 1952] in the case of orthorhombic crystals.

While the bulk of the lower mantle is isotropic [*Meade et al.*, 1995], anisotropic regions are of particular interest, because they occur within the D'' layer [*Vinnik et al.*, 1995; *Matzel et al.*, 1996; *Kendall and Silver*, 1996; *Garnero and Lay*, 1997], and because observations of anisotropy contain, in principle, information about mantle flow [*Park and Yu*, 1993]. In monophase aggregates, anisotropy arises through Lattice Preferred Orientation (LPO). LPO may be produced when the aggregate is subjected to deviatoric stresses, as in a convecting system.

In order to estimate the properties of anisotropic mono-phase aggregates in the deep earth, we follow *Karato* [1997] in making the following assumptions: 1) mantle flow in dynamical boundary layers is primarily horizontal; this is likely to be a good approximation in D'' 2) lower mantle minerals contain a dominant slip plane and slip direction which largely controls their rheology 3) the dominant slip planes and directions can be estimated on the basis of ambient pressure data and/or analog materials and 4) the texture is fully developed (perfect): slip planes and directions are parallel to the flow plane and direction, respectively. The latter assumption means that we will be examining upper limits to the anisotropy of aggregates. In general, alignment of all grains of the aggregate with the flow will not be perfect, and the anisotropy will be correspondingly reduced.

Table 1. Dominant Slip Planes and Slip Directions

Phase	Slip Plane	Slip Direction
Perovskite[1]	(010)	[100]
Periclase[2]	{110}	< 111 >
Stishovite[3]	{101}	< 101 >
$CaCl_2$-type	(101)	$[\bar{1}01]$
Columbite-type	(101)	$[\bar{1}01]$

References: 1, [*Karato et al.*, 1995]; 2, [*Chin and Mammel*, 1973]; 3, [*Ashbee and Smallman*, 1963]. Deformation mechanisms in $MgSiO_3$ perovskite, and stishovite are taken from experiments on isostructural analogs: $CaTiO_3$ perovskite and TiO_2 rutile, respectively. Deformation of the silica phases is assumed to be controlled by the direction of the chains of edge-sharing octahedra which are parallel to the c-axis in all three phases.

There are two cases to consider: 1) azimuthal anisotropy and 2) transverse anisotropy. In the first case, the flow is coherent over a length scale that is large compared with the region sampled by the seismic wave. In this case, assuming perfect alignment, the elasticity of the aggregate is that of a single crystal. In the second case, the flow is still horizontal, but is azimuthally variable over the region sampled. This situation may occur in the vicinity of stationary points in the flow that will exist at centers of convergence (upwelling) or divergence (downwelling). In this case, slip planes will be horizontal, but slip directions may be approximately evenly distributed over the azimuthal direction. Transverse anisotropy may also have a rheological origin: if the deformation mechanism has a dominant slip plane, but no dominant slip direction, transverse anisotropy will result. The assumed dominant slip planes and slip directions for the phases considered here are summarized in Table 1.

The elastic constants of an azimuthally anisotropic aggregate are those of the single crystal, but rotated into the coordinate system of the flow. We define a crystallographic coordinate system (x) and a laboratory or mantle coordinate system (x') in which x'_3 defines the vertical and coincides with the normal to the flow plane and x'_1 coincides with the flow direction (Fig. 1). The rotation matrix relates the two coordinate systems:

$$a_{ij} = cos(\theta_{i'j}) \tag{7}$$

where $\theta_{i'j}$ is the angle between x'_i and x_j. The elastic constant tensor of the azimuthally anisotropic aggregate is then

$$c'_{ijkl} = a_{im}a_{jn}a_{ko}a_{lp}c_{mnop} \tag{8}$$

where c_{mnop} is the elastic constant tensor in the crystallographic coordinate system [*Nye*, 1985].

In the case of transverse anisotropy, the aggregate is isotropic within the flow plane. We define a coordinate system x'' for which x''_3 coincides with x'_3, and x''_1 is related to x'_1 by the azimuthal angle ϕ (Fig. 1). The primed and double-primed coordinate systems are related by the rotation matrix:

$$\mathbf{b} = \begin{pmatrix} \cos(\phi) & \sin(\phi) & 0 \\ -\sin(\phi) & \cos(\phi) & 0 \\ 0 & 0 & 1 \end{pmatrix} \tag{9}$$

The elastic constant tensor of the transversely isotropic aggregate is

$$c''_{ijkl} = \frac{1}{2\pi}\int_0^{2\pi} b_{im}b_{jn}b_{ko}b_{lp}c'_{mnop}d\phi \tag{10}$$

The elastic constants in this case will always have hexagonal symmetry.

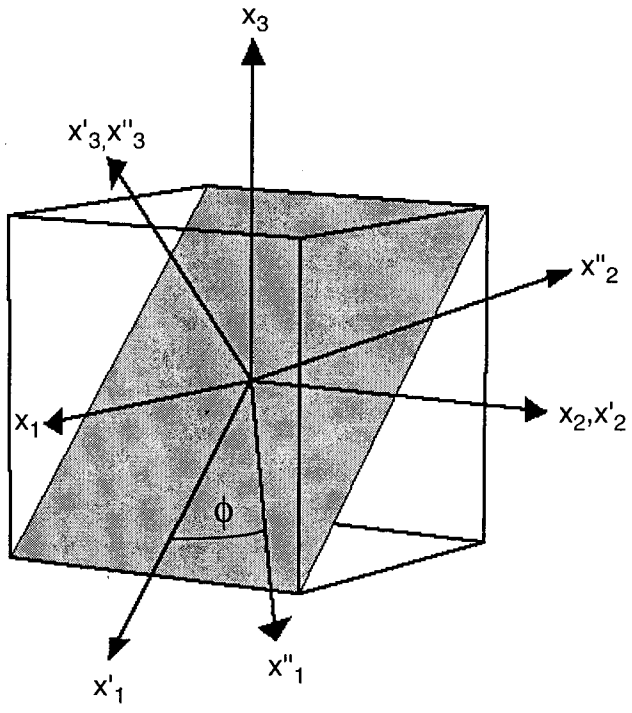

Figure 1. Coordinate systems used in the analysis of anisotropic aggregates. The example shown corresponds to stishovite: (101) is the slip plane and $[10\bar{1}]$ the slip direction.

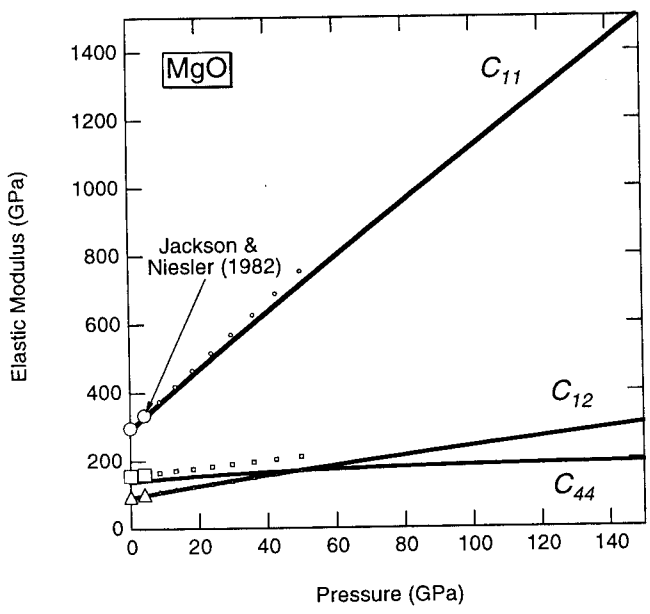

Figure 2. Elastic constants of periclase according to theory [*Karki et al.*, 1997a] (lines) and experiment [*Jackson and Niesler*, 1982] large symbols. Small symbols represent a linear extrapolation of the experimental results beyond the maximum pressure of the measurements (3 GPa).

To characterize the anisotropy of transversely anisotropic aggregates we consider the ratio PH/PV of the velocity of horizontally to vertically propagating P-waves, and the ratio SH/SV of the velocity of horizontally to vertically polarized shear waves propagating in the horizontal plane. For azimuthally anisotropic aggregates, we consider the shear wave splitting $S_{\parallel}/S_{\perp}$, the ratio of velocities of vertically propagating shear waves, one polarized in the flow direction, the other perpendicular to it. The velocities are calculated from an equivalent form of the Cristoffel Equation (3)

$$\rho V^2 = c_{ijkl} n_i w_j n_k w_l \qquad (11)$$

where $\vec{w}$ is the polarization direction.

4. RESULTS

4.1. Elastic Constants

First principles elastic constants of the the orthorhombic *Pbnm* structure of $MgSiO_3$ perovskite, the B1 structure of MgO (periclase), and stishovite are in excellent agreement with experimental data (Figs. 2-4, Tables 2,3). The agreement with observation substantially surpasses that achieved by previous theoretical approaches including semi-empirical ionic potentials [*Matsui et al.*,

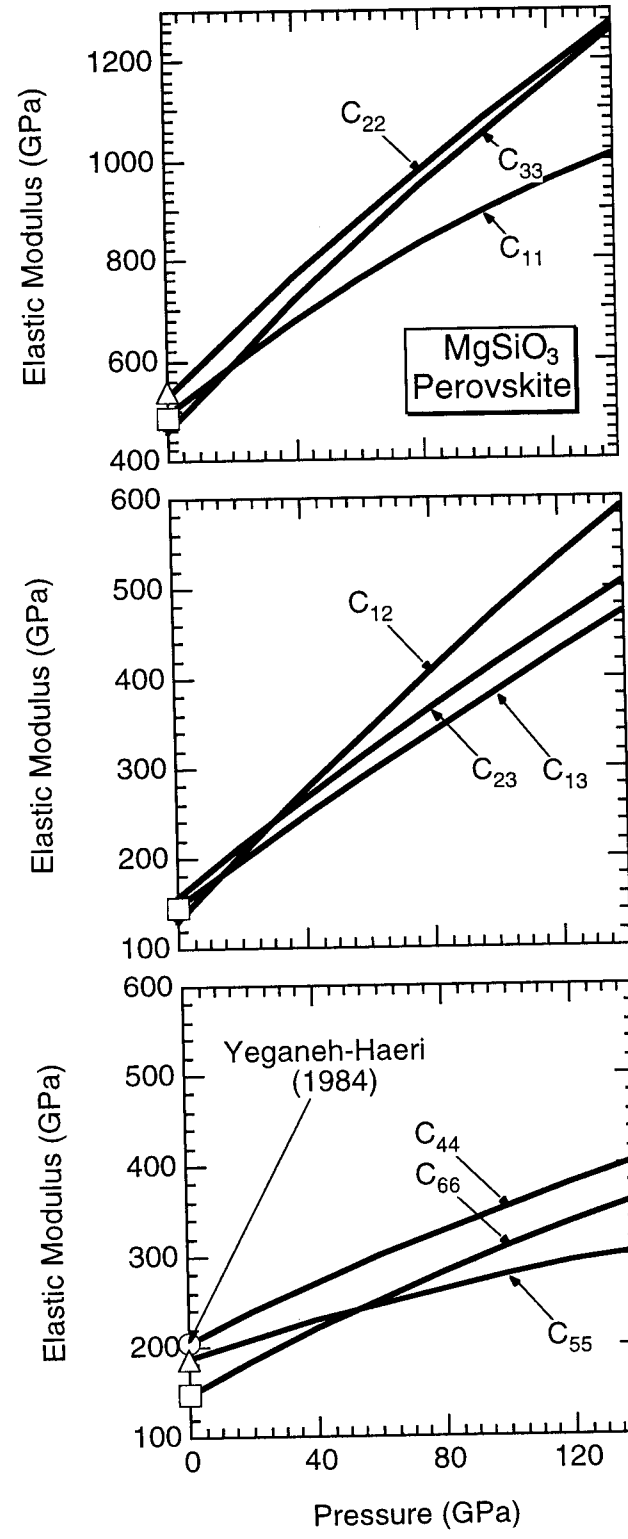

Figure 3. Elastic constants of $MgSiO_3$ perovskite according to theory [*Karki et al.*, 1997b] (lines) and experiment [*Yeganeh-Haeri*, 1994] symbols: c_{11}, c_{12}, c_{44} (○); c_{22}, c_{13}, c_{55} (△); c_{33}, c_{23}, c_{66} (□).

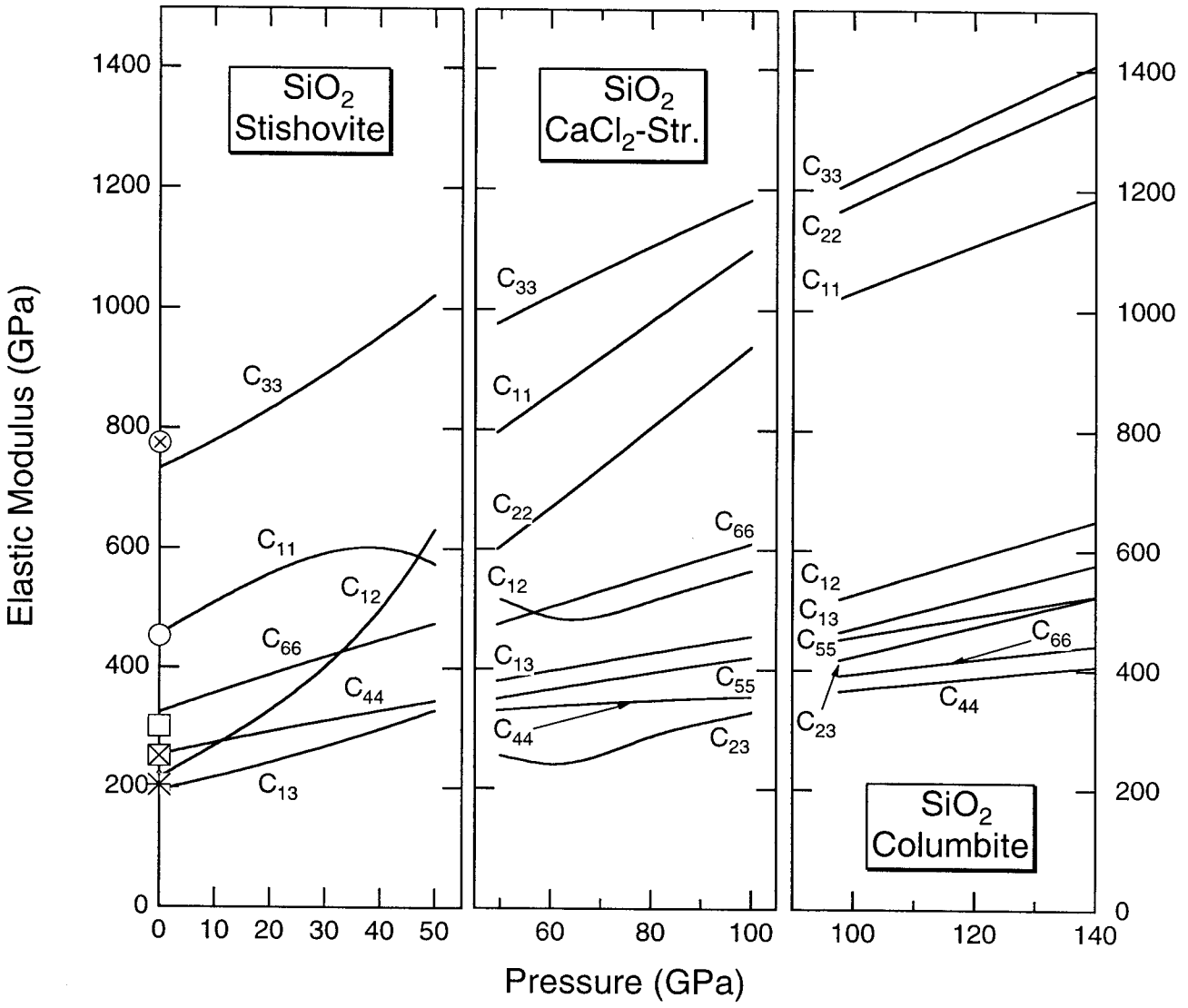

Figure 4. Theoretical predictions of the elastic constants of the three phases of SiO_2 [*Karki et al.*, 1997c] (lines) compared with experimental measurements of stishovite [*Weidner et al.*, 1982] symbols: c_{11} (o); c_{33} (⊗); c_{12} (△); c_{13} (*); c_{44} (×); c_{66} (□).

1987] or *ab initio* potential induced breathing methods [*Cohen*, 1987; *Isaak et al.*, 1990]. The better agreement is not surprising. Unlike previous approaches, the first principles calculations make no *a priori* assumptions regarding the nature of the electronic structure or bonding. The fact that the pseudopotential method predicts elastic constants in much better agreement with experiment than the modified electron gas model indicates that covalent or angle-dependent forces are important for understanding the elasticity of perovskite.

We attribute remaining differences between theory and experiment to 1) temperature; ambient temperature (300 K) is expected to reduce elastic constants by 2-6 % relative to the athermal (0 K, no zero point motion) values calculated theoretically [*Anderson and Isaak*, 1995] 2) the LDA; comparison between LAPW and experiment indicates that this error is of the order of 2 % in volume and 3 % in bulk modulus [*Mehl et al.*, 1988; *Karki et al.*, 1997a] and 3) the pseudopotential approximation. For the particular pseudopotentials used in this study, the latter two errors partially cancel one another. While the LDA tends to underestimate lattice parameters and overestimate elastic constants, the Q_c-tuning pseudopotentials tend to overexpand the lattice

Table 2. Moduli, M_0, and their first pressure derivatives M_0' at zero pressure from first principles theory.

	$MgSiO_3$ Perovskite[1]		MgO Periclase[2]	
	M_0 (GPa)	M_0'	M_0 (GPa)	M_0'
c_{11}	493	5.15	291	9.00
c_{22}	523	6.56		
c_{33}	460	6.70		
c_{12}	135	3.33	90.0	1.91
c_{13}	145	2.55		
c_{23}	158	2.73		
c_{44}	201	1.98	135	1.30
c_{55}	183	1.44		
c_{66}	147	1.91		

References: 1, [*Karki et al.*, 1997b]; 2, [*Karki et al.*, 1997a]. Moduli and pressure derivatives are from third-order Eulerian finite strain fits to the first principles results.

relative to all electron LDA calculations by a similar amount. The maximum deviation between theory and experiment is 11 % in the case of c_{44} of periclase. The RMS deviations of the elastic constants between theory and experiments are 5 %, 7 % and 4 %, respectively for perovskite, periclase and stishovite.

Theory predicts that silica undergoes two phase transformations within the pressure regime of the lower mantle [*Karki et al.*, 1997d]. Stishovite is predicted to transform to a $CaCl_2$ type structure at 47 GPa, in essentially perfect agreement with all electron calculations and experiment [*Cohen*, 1992; *Kingma et al.*, 1995]. This transition involves a shear-mode softening ($c_{11}-c_{12} \rightarrow 0$), which has a major effect on the acoustic velocities of isotropic and anisotropic silica-containing aggregates. The phase of silica relevant for understanding the base of the lower mantle is isostructural with columbite (and α-PbO_2) to which the $CaCl_2$-type phase is predicted to transform at 98 GPa. This prediction is consistent with recent experimental data [*Kingma et al.*, 1996].

The predicted elastic constants of $MgSiO_3$ perovskite, periclase and SiO_2 columbite at the pressure of the core-mantle boundary are reported in Table 4.

4.2. Velocities of Isotropic Aggregates

Theory predicts that the elastic wave velocities of mono-phase aggregates of perovskite lie in between those of its constituent oxides (Figs. 5,6). The P- and S-wave velocities (V_P and V_S, respectively) of the columbite structure exceed those of perovskite by 6 and 9 % respectively and those of periclase by 9 and 11 % respectively at pressures corresponding to the base of the mantle.

Silica is the seismically fastest material throughout the pressure regime of the lower mantle except near 47 GPa, where it is the slowest. This unusual behavior is caused by the phase transition from stishovite to the $CaCl_2$-type structure. This phase transition involves a shear-mode softening, and a rapid decrease

Table 3. Moduli, M_0, and their first and second pressure derivatives M_0', M_0'' at zero pressure from first principles theory[1].

	SiO_2 Stishovite			SiO_2 $CaCl_2$-type	SiO_2 Columbite-type	
	M_0 (GPa)	M_0'	M_0'' (GPa^{-1})	M (GPa)	M_0 (GPa)	M_0'
c_{11}	456	5.32	0.000	794	557	5.90
c_{22}				602	624	6.78
c_{33}	734	4.31	0.028	988	640	7.04
c_{12}	216	5.32	0.000	516	196	3.57
c_{13}	195	2.03	0.011	382	181	3.16
c_{23}				255	155	2.91
c_{44}	254	2.09	(-0.012)	332	230	1.88
c_{55}				350	245	2.59
c_{66}	325	3.30	(-0.017)	475	237	2.08

References: 1, [*Karki et al.*, 1997c]. Moduli and pressure derivatives are from Eulerian finite strain fits to the theoretical results, except for $CaCl_2$ for which we tabulate values of the elastic constants at a pressure of 50 GPa. We used third-order fits for columbite and c_{44} and c_{66} of stishovite and fourth order for c_{33} and c_{13} of stishovite. Second derivatives in parentheses are from third order fits. The pressure dependence of c_{11} and c_{12} of stishovite is represented by $(c_{11}+c_{12})/2 = 336 + 5.32P$ and $(c_{11}-c_{12})/2 = 120[1-(P/47)^{3.5}]$, where P is pressure in GPa.

Table 4. Elastic Constants at $P = 136$ GPa.

	$MgSiO_3$ Perovskite	Periclase	SiO_2 Columbite
c_{11}	996	1388	1171
c_{22}	1250		1341
c_{33}	1237		1391
c_{12}	577	286	639
c_{13}	463		566
c_{23}	495		513
c_{44}	398	192	403
c_{55}	300		518
c_{66}	355		437

in V_S and V_P over a narrow pressure interval. The lower bound on V_S vanishes at the transition while the Hashin-Shtrikman average value decreases by 50 % between 40 and 47 GPa. Once the transition is complete, velocities return to values similar to those far from the transition instantaneously, at a single pressure.

The P- and S-wave velocities of silica exhibit another discontinuous change at the transition from the $CaCl_2$- to the columbite-type phase at 98 GPa (2210 km depth). The P-wave velocity increases slightly at this transition (by 1 %) and the S-wave velocity decreases by a similar amount.

4.3. Single Crystal Anisotropy

The single crystal anisotropy of all three materials is predicted to depend strongly on pressure (Fig. 7). Not only do the magnitudes of P- and S-wave anisotropy change significantly over the pressure regime of the lower mantle, but the sense of anisotropy changes as well. In perovskite, the direction of slowest P-wave propagation is [001] at 0 GPa, but [100] at 140 GPa. This behavior can be understood in terms of the elastic constants and reflects the fact that of the longitudinal elastic moduli (c_{ii} for $i \leq 3$), c_{33} is the least at ambient pressure but c_{11} is the least at 140 GPa.

Periclase shows a larger change in anisotropy. The anisotropy is predicted to decrease with pressure initially, vanishing at 20 GPa before increasing again at high pressures. This behavior is not related to a structural or phase transition but results from the interchange of fast and slow directions as pressure increases. For example, the fast direction of P-wave propagation at zero pressure [111], becomes the slow direction above 20 GPa. Similar interchanges in the fast and slow directions of S-wave propagation and polarization occur at the same pressure. In a cubic material this behavior can be understood in terms of a single combination of elastic constants $c_{11} - c_{12} - 2c_{44}$ which changes sign at 20 GPa and can be shown to determine P- and S-wave azimuthal and polarization anisotropy. This quantity is negative at ambient pressures but becomes positive at higher pressures because c_{11} depends on pressure much more strongly than c_{12} or c_{44}.

Silica shows the largest anisotropy and the largest change in anisotropy with pressure. The azimuthal S-wave anisotropy of stishovite changes by nearly a factor of 2 between 0 and 40 GPa, rising to a value of 190 % near the transition to the $CaCl_2$ structure. The anisotropy of the $CaCl_2$ structure is also large (60 % S-wave azimuthal anisotropy at 60 GPa). The anisotropy of the columbite structure is substantially smaller, but still greater than that of perovskite in the D″ layer.

4.4. Anisotropic Aggregates

Transverse and azimuthal anisotropy depend strongly on pressure so that measurements at ambient conditions provide little guidance as to the anisotropy at the base of the lower mantle (Fig. 8). For example, in periclase, the P- and S-wave anisotropies reverse sign at 20 GPa. This sign reversal and the vanishing of the single crystal anisotropy at the same pressure have the same origin; namely a change in sign of $c_{11} - c_{12} - 2c_{44}$. The magnitude of transverse P- and S-wave anisotropy in periclase

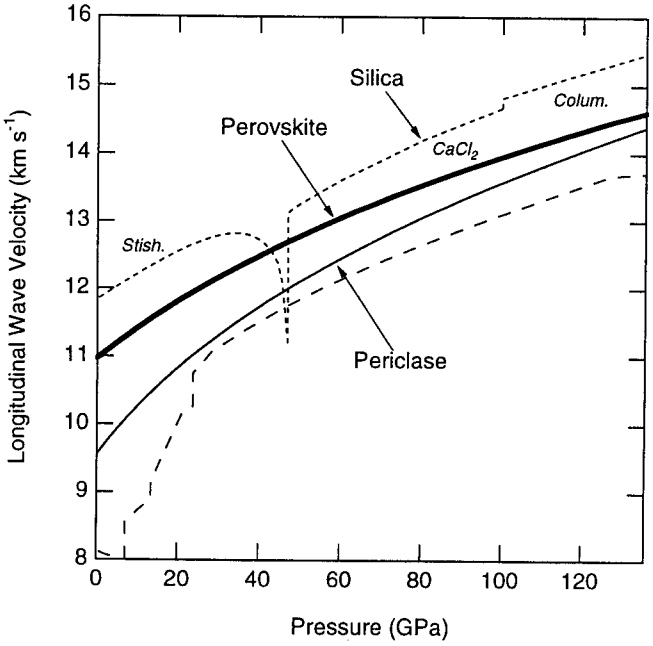

Figure 5. Longitudinal (P) wave velocity of isotropic mono-phase aggregates compared with the P-wave velocity of the lower mantle (long dashed line).

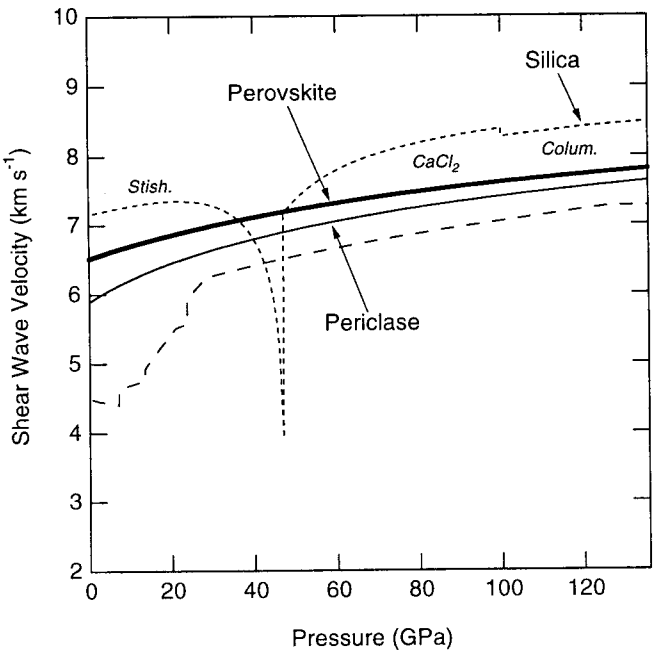

Figure 6. Shear (S) wave velocity of isotropic mono-phase aggregates compared with the S-wave velocity of the lower mantle (long dashed line).

at the base of the mantle are approximately 2 % and 6 %, respectively. The $S_{||}/S_{\perp}$ anisotropy is substantially larger and reaches a value of 16 % at the base of the mantle.

The anisotropy of perovskite aggregates also depends strongly on pressure. The SH/SV anisotropy is essentially zero at ambient pressure but reaches -9 % at the base of the mantle. The slower SH velocity results from the much weaker dependence of c_{55} on pressure and its smaller value at high pressure compared with that of c_{44} and c_{66}. The $S_{||}/S_{\perp}$ anisotropy reflects the ratio of c_{66} to c_{44} and varies from -15 % at ambient pressure to -5 % at the base of the mantle. Only the PH/PV anisotropy changes by a relatively small amount with pressure, from -4 % to -6 %. PH/PV anisotropy is largely controlled by the difference between c_{22}, corresponding to propagation along the b-axis, the vertical direction for the slip plane assumed here, and the average of c_{11} and c_{33}.

Silica aggregates generally show the largest variation with pressure. This is due to the two phase transitions, and to the anomalous behavior of stishovite and $CaCl_2$ in the vicinity of the phase transition at 47 GPa. Shear mode softening in the stishovite phase leads to the largest magnitudes of S-wave anisotropy of any phase studied here, up to -28 % in $S_{||}/S_{\perp}$. Although large, this anisotropy is substantially less than the single-crystal S-wave anisotropy. The reason for the difference is that the dominant slip plane does not coincide with the plane of shear-mode softening: the phase transition is driven by a rotation of the octahedra in the $a-b$ plane (001) while experiments on rutile indicate that {101} are the dominant slip planes.

5. DISCUSSION

5.1. The Lower Mantle

Our results have allowed us to compare, for the first time, the P- and S- wave velocities of major mantle phases with observed seismological properties of the lower mantle. Comparison with the isotropic homogeneous (radial) structure of the lower mantle shows that the P- and S-wave velocity profiles of $MgSiO_3$ perovskite are nearly parallel to those of the lower mantle [*Karki et al.*, 1997b]. Further, the velocities of this mineral are similar in magnitude to those of the lower mantle. Theoretical P- and S-wave velocities are higher by 6 and 8 %, respectively, than those observed seismologically. We attribute the differences between theoretical and seismological velocities to 1) the effect of Fe, which is expected to lower the velocities of perovskite by 1-2 % 2) the high temperatures of the lower mantle which are expected to reduce velocities by several percent relative to the athermal values determined theoretically and 3) the possible presence of other phases in the lower mantle including magnesiowüstite, $CaSiO_3$ perovskite, silica, and garnet.

This result represents an important test of the prevailing view that Mg-rich silicate perovskite is the most abundant mineral in the lower mantle. This hypothesis has been supported in the past by only a limited subset of the observed seismological properties of the lower mantle: the density and bulk modulus [*Jeanloz and Knittle*, 1989; *Bukowinski and Wolf*, 1990; *Stixrude et al.*, 1992; *Bina and Silver*, 1997]. Our results show for the first time that those properties which are most sensitively measured by seismic observations, V_P and V_S, are also consistent with a perovskite rich lower mantle. This is also significant because V_P and V_S are expected to be more sensitive to bulk composition and mineral structure than are density and bulk modulus.

The predicted velocities of periclase indicate that magnesiowüstite will have very low seismic velocities in the lower mantle. The effect of iron on the P- and S-wave velocities of magnesiowüstite is expected to be large both because of its large effect on the density and because magnesiowüstite is expected to be enriched in

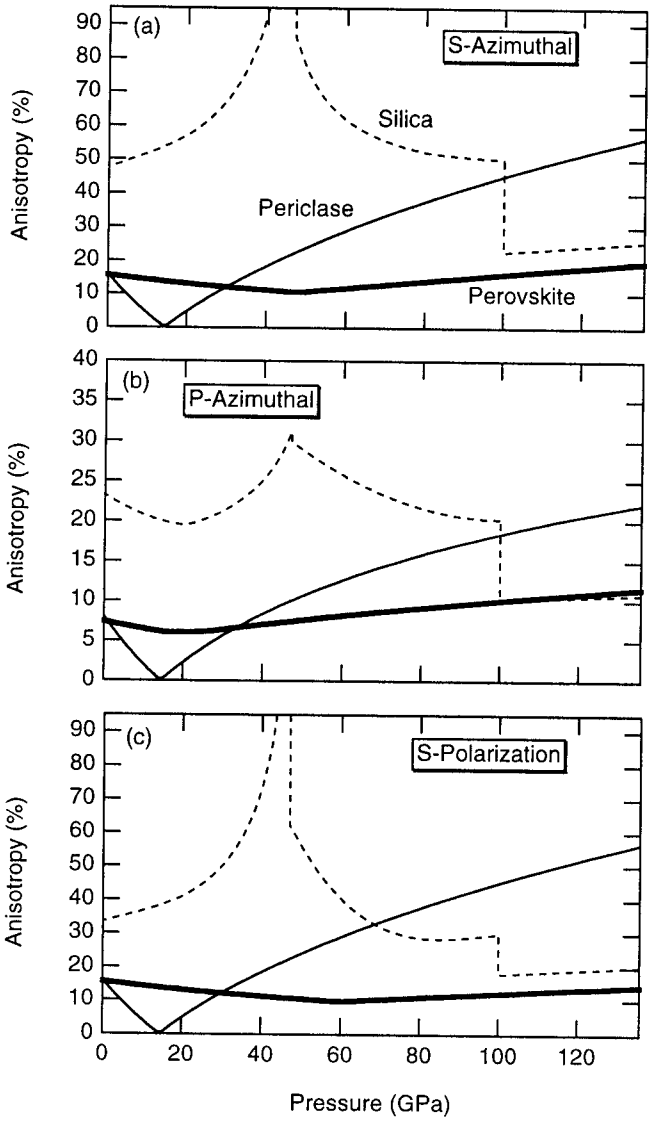

Figure 7. Single crystal anisotropy of $MgSiO_3$ perovskite (bold lines), periclase (light solid lines), and silica (dashed lines): a) azimuthal anisotropy of S-waves b) azimuthal anisotropy of P-waves c) maximum polarization anisotropy.

iron compared with the bulk lower mantle. Existing data indicates that iron may lower the P- and S-wave velocities of magnesiowüstite by 6-12 and 8-16 %, respectively, relative to that of periclase. These estimates, primarily based on ambient pressure data are uncertain because 1) there are no experimental or theoretical results on the elasticity of Fe-bearing magnesiowüstites at high pressure 2) phase transitions in end-member FeO suggest that high pressure behavior may differ significantly from that at ambient conditions and 3) uncertainties in measured quantities such as the magnesiowüstite-perovskite Fe partition coefficient (K_{pv-mw}). and 4) uncertainties in the iron content of the lower mantle. Our estimates are based on an assumed bulk iron content of the lower mantle $X_{Fe} = \frac{Fe}{Mg+Fe} = 8-12$ %, and a range of values for the partition coefficient $K_{pv-mw} = 1/6 - 1/3$.

The very low seismic wave velocities of magnesiowüstite suggested by our results promise a resolution of the long-standing question of the major element bulk composition of the lower mantle. Despite the remaining

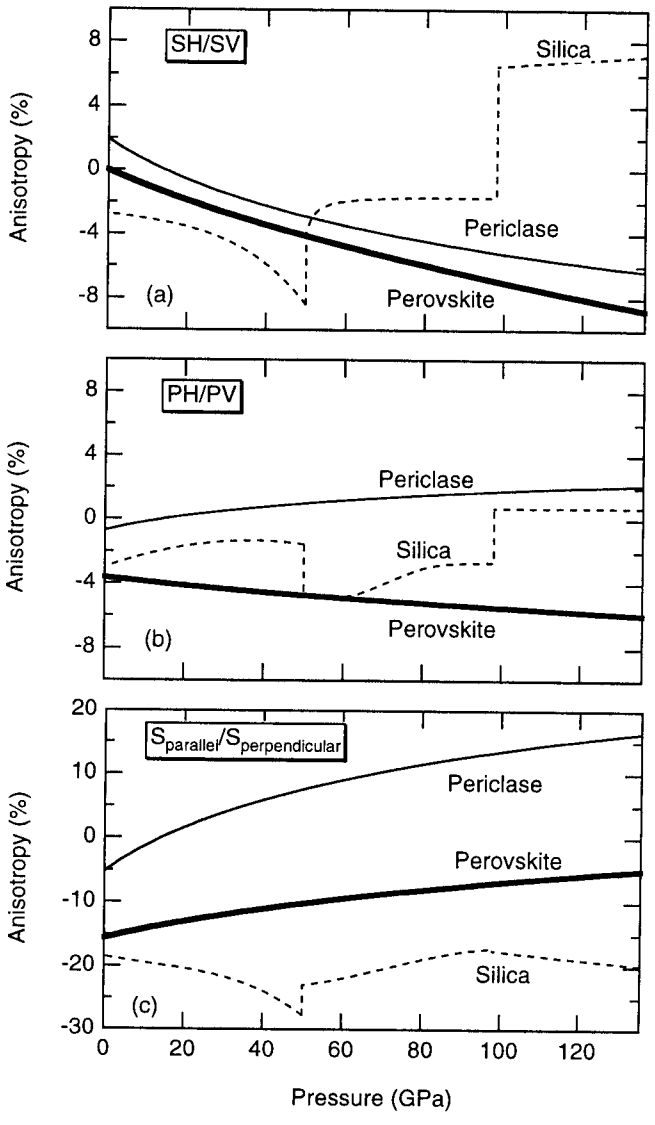

Figure 8. Anisotropy of mono-phase aggregates. a) $SH/SV - 1$ b) $PH/PV - 1$ and c) $S_{\parallel}/S\perp - 1$. Bold lines are for $MgSiO_3$ perovskite, light solid lines for periclase and dashed lines for silica.

uncertainties in the effect of Fe, it seems clear that the P- and S-wave velocities of magnesiowüstite will be substantially lower than that of perovskite at lower mantle conditions; the S-wave velocities may differ by 15 %. In contrast, the density of these two phases differ by only 2.5 % on average throughout the lower mantle. This small difference, combined with the fact that the density is less well determined seismologically than either V_P or V_S accounts for the difficulty of resolving the question of lower mantle composition on the basis of density alone. The relatively large difference in V_S and V_P between perovskite and magnesiowüstite reflects the sensitivity of the shear modulus to crystal structure and bulk composition.

The seismic wave velocities of silica remain significantly higher than those of the lower mantle throughout most of the relevant pressure regime (by as much as 20 % in V_S). However, for pressures near 50 GPa (1200 km depth), the athermal S-wave velocity of silica is 20 % smaller than that of the lower mantle. The unusual velocity structure associated with the stishovite to $CaCl_2$ transition - a rapid and large decrease in velocities with pressure (depth) followed by a sudden and equally large increase - is capable of reflecting seismic energy in the frequency band typically observed seismically. This presents the possibility that even small amounts of silica in the lower mantle may be seismically detectable. We have found that a lower mantle with as little as 2 volume percent silica would show significant reflectivity at the depth of the phase transition. This may provide an explanation of at least a subset of seismically reflective features within the lower mantle at depths of 710-785 km, 920 km, and 1180 km [*Karki et al.*, 1997c].

5.2. *Anisotropy in D″*

Hypotheses concerning the origin of anisotropy in D″ have been difficult to test because of our lack of knowledge of the elastic constants of possible D″ constituents. Our results allow us to test the hypothesis that the anisotropy originates in lattice preferred orientation. This hypothesis is motivated by the expected, nearly mono-mineralic composition of the lower mantle (75-100 volume % Mg-rich silicate perovskite) and by the expectation that deviatoric stress due to mantle flow are concentrated in the mantle's dynamical boundary layers.

We find that perovskite, periclase, and silica all have anisotropy of sufficient magnitude to explain seismological observations. Observations show that the anisotropy in D″ is typically less than 2 %, significantly smaller than the upper bounds on aggregate anisotropy found here (6-8 %, Fig. 8).

Our results show that lattice-preferred orientation is likely to produce anisotropy such that SV is faster than SH. Mono-phase aggregates of both perovskite and periclase show this sense of anisotropy. The columbite phase of silica has the opposite sense of anisotropy, but is unlikely to be a major constituent of D″ because of its very high velocities.

Seismological studies find anisotropy of the same sense ($SV > SH$) in some regions of D″ [*Pulliam and Sen*, 1998]. In these regions, theory indicates that lattice preferred orientation of a perovskite dominated aggregate is responsible for the observations.

In other regions of D″, SH is found to be faster than SV [*Kendall and Silver*, 1996; *Garnero and Lay*, 1997]. In these regions, theory supports explanations based on shape preferred orientation. This class of explanations is much more difficult to test at present because it relies on elastic constants of materials that are not yet measured or predicted. For example, one possible origin of lamellar structures in D″ which may be able to explain the observations are chemical reactions between mantle and core [*Knittle and Jeanloz*, 1991]. Aside from silica, the elasticity of the reaction products are unknown.

6. CONCLUSIONS

Modern first principles methods are now capable of realistic predictions of the elastic constants of complex silicates such as perovskite. Although independent of experiment, we have shown that these methods are able to reproduce even subtle features such as elastic anisotropy with good accuracy. We note that it is possible to extend these methods to high temperatures, although we have not done so here. Modern electronic structure theory thus promises an ideal complement to the experimental approach, and the ability to determine the elasticity and anisotropy of major constituents throughout the pressure and temperature regime of the earth's mantle.

Investigation of the deformation mechanisms of high pressure phases will be another important avenue of future research. This knowledge is critical for understanding the development of lattice preferred and in some cases, shape preferred orientation due to mantle flow. This area of investigation is now accessible to theory and experiment.

Acknowledgments. This work supported by the National Science Foundation under grant EAR-9628199.

REFERENCES

Anderson, O. L., and D. G. Isaak, Elastic constants of mantle minerals at high temperature. In T. J. Ahrens, editor, *Mineral Physics and Crystallography: A Handbook of Physical Constants*, pages 64–97. American Geophysical Union, Washington, DC, 1995.

Ashbee, K. H. G., and R. E. Smallman, The plastic deformation of titanium dioxide single crystals. *Proceedings of the Royal Society of London, Series A, 274*, 195–205, 1963.

Bass, J. D., Elasticity of minerals, glasses, and melts. In T. J. Ahrens, editor, *Mineral Physics and Crystallography: A Handbook of Physical Constants*, pages 45–63. American Geophysical Union, Washington, DC, 1995.

Bina, C. R., and P. G. Silver, Bulk sound travel times and implications for mantle composition and outer core heterogeneity. *Geophysical Research Letters, 24*, 499–502, 1997.

Bukowinski, M. S. T., and G. H. Wolf, Thermodynamically consistent decompression - implications for lower mantle composition. *Journal of Geophysical Research, 95*, 12583–12593, 1990.

Chen, G. L., B. S. Li, and R. C. Liebermann, Selected elastic moduli of single-crystal olivines from ultrasonic experiments to mantle pressures. *Science, 272*, 979–980, 1996.

Chin, G. Y., and W. L. Mammel, A theoretical examination of the plastic deformation of ionic crystalsii. analysis of uniqcial deformation and axisymmetric flow for slip on $(110)\langle 100\rangle$ and $(100)\langle 110\rangle$ systems. *Metallurgical Transactions, 4*, 335–340, 1973.

Cohen, R. E., Elasticity and equation of state of $MgSiO_3$ perovskite. *Geophysical Research Letters, 14*, 1053–1056, 1987.

Cohen, R. E., Bonding and elasticity of stishovite SiO_2 at high pressure: linearized augmented plane wave calculations. *American Mineralogist, 76*, 733–742, 1991.

Cohen, R. E., First-principles predictions of elasticity and phase transitions in high pressure SiO_2 and geophysical implications. In Y. Syono and M. H. Manghnani, editors, *High-Pressure Research: Applications to Earth and Planetary Sciences*, pages 425–431. TERRAPUB, Tokyo, 1992.

da Silva, C., L. Stixrude, and R. M. Wentzcovitch, Elastic constants and anisotropy of forsterite at high pressure. *Geophysical Research Letters, 24*, 1963–1966, 1997.

Duffy, T. S., C. S. Zha, R. T. Downs, and H. K. Mao et al., Elasticity of forsterite to 16 gpa and the composition of the upper mantle. *Nature, 378*, 170–173, 1995.

Garnero, E. J., and T. Lay, Lateral variations in lowermost mantle shear wave anisotropy beneath the north pacific and alaska. *Journal of Geophysical Research, 102*, 8121–8135, 1997.

Gunnarsson, O., and B. I. Lundqvist, Exchange and correlation in atoms, molecules, and solids by the spin-density-functional formalism. *Physical Review B, 13*, 4274–4298, 1976.

Hashin, Z., and S. Shtrikman, A variational approach to the theory of the elastic behavior of polycrystals. *Journal of the Mechanics and Physics of Solids, 10*, 343–352, 1962.

Hill, R., The elastic behavior of a crystalline aggregate. *Proceedings of the Physical Society, London, 65A*, 349–354, 1952.

Hohenberg, P., and W. Kohn, Inhomogeneous electron gas. *Physical Review, 136*, B864–B871, 1964.

Isaak, D. G., R. E. Cohen, and M. E. Mehl, Calculated elastic constants and thermal properties of MgO at high pressures and temperatures. *Journal of Geophysical Research, 95*, 7055–7067, 1990.

Jackson, I., and H. Niesler, The elasticity of periclase to 3 gpa and some geophysical implications. In S. Akimoto and M. H. Manghnani, editors, *High-Pressure Research in Geophysics*, pages 93–133. Center for Academic Publications, Tokyo, 1982.

Jeanloz, R., and E. Knittle, Density and composition of the lower mantle. *Philosophical Transactions of the Royal Society of London Series A, 328*, 377–389, 1989.

Karato, S., S. Zhang, and H.-R. Wenk, Superplasticity in earth's lower mantle: evidence from seismic anisotropy and rock physics. *Science, 270*, 458–461, 1995.

Karki, B. B., L. Stixrude, S. J. Clark, M. C. Warren, G. J. Ackland, and J. Crain, Structure and elasticity of MgO at high pressure. *American Mineralogist, 82*, 51–60, 1997a.

Karki, B. B., L. Stixrude, S. J. Clark, M. C. Warren, G. J. Ackland, and J. Crain, Elastic properties of orthorhombic $MgSiO_3$ perovskite at lower mantle pressures. *American Mineralogist, 82*, 635–638, 1997b.

Karki, B. B., L. Stixrude, M. C. Warren, G. J. Ackland, and J. Crain, *Ab initio* elasticity of three high-pressure polymorphs of silica. *Geophysical Research Letters, 24*, 3269–3272, 1997c.

Karki, B. B., M. C. Warren, L. Stixrude, G. J. Ackland, and J. Crain, *Ab initio* studies of high-pressure structural transformations in silica. *Physical Review B, 55*, 3465–3471, 1997d.

Kendall, J. M., and P. G. Silver, Constraints from seismic anisotropy on the nature of the lowermost mantle. *Nature, 381*, 409–412, 1996.

Kiefer, B., L. Stixrude, and R. M. Wentzcovitch, Elastic constants and anisotropy of Mg_2SiO_4 spinel at high pressure. *Geophysical Research Letters, 24*, 2841–2844, 1997.

Kingma, K. J., R. E. Cohen, R. J. Hemley, and H. K. Mao, Transformation of stishovite to denser phase at lower-mantle pressures. *Nature, 374*, 243–245, 1995.

Kingma, K., H. K. Mao, and R. J. Hemley, Synchtrotron x-ray diffraction of SiO_2 to multimegabar pressures. *High Pressure Research, 14*, 363–374, 1996.

Knittle, E., and R. Jeanloz, Earth's core-mantle boundary - results of experiments at high pressures and temperatures. *Science, 251*, 1438–1443, 1991.

Kohn, W., and L. J. Sham, Self-consistent equations including exchange and correlation effects. *Physical Review, 140*, A1133–A1138, 1965.

Kresse, G., J. Hafner, and R. J. Needs, Optimized norm-conserving pseudopotentials. *Journal of Physics - Condensed Matter, 4*, 7451–7468, 1992.

Lin, J. S., Q. Qteish, M. C. Payne, and V. Heine, Optimised and transferable non-local separable ab-initio pseudopotentials. *Physical Review B, 47*, 4174–4180, 1993.

Lundqvist, S., and N. H. March, *Theory of the Inhomogeneous Electron Gas*. Plenum Press, London, 1987.

Matsui, M., M. Akaogi, and T. Matsumoto, Computational

model of the structural and elastic properties of the ilmenite and perovskite phases of $MgSiO_3$. *Physics and Chemistry of Minerals, 14*, 101–106, 1987.

Matzel, E., M. K. Sen, and S. P. Grand, Evidence for anisotropy in the deep mantle beneath alaska. *Geophysical Research Letters, 23*, 2417–2420, 1996.

Meade, C., P. G. Silver, and S. Kaneshima, Laboratory and seismological observations of lower mantle isotropy. *Geophysical Research Letters, 22*, 1293–1296, 1995.

Mehl, M. J., R. E. Cohen, and H. Krakauer, Linearized augmented plane wave electronic structure calculations for MgO and CaO. *Journal of Geophysical Research, 93*, 8009–8022, 1988.

Meister, R., and L. Peselnick, Variational method of determining effective moduli of polycrystals with tetragonal symmetry. *Journal of Applied Physics, 37*, 4121–4125, 1966.

Monkhurst, H. J., and J. D. Pack, Special points for brillouin-zone integrations. *Physical Review B, 13*, 5188–5192, 1976.

Nielsen, O. H., and R. Martin, Quantum mechanical theory of stress and force. *Physical Review B, 32*, 3780–3791, 1985.

Nye, J. F., *Physical Properties of Crystals: Their Representation by Tensors and Matrices.* Oxford, Oxford, UK, 2 edition, 1985.

Park, J., and Y. Yu, Seismic determination of elastic anisotropy and mantle flow. *Science, 261*, 1159–1162, 1993.

Pickett, W. E., Pseudopotentials in condensed matter systems. *Comp. Phys. Rep., 9*, 114–197, 1989.

Pulliam, J., and M. K. Sen, Seismic anisotropy in the core-mantle transition zone. *Geophysical Journal International*, in press, 1998.

Stixrude, L., and R. E. Cohen, Stability of orthorhombic $MgSiO_3$-perovskite in the earth's lower mantle. *Nature, 364*, 613–161, 1993.

Stixrude, L., R. J. Hemley, Y. Fei, and H. K. Mao, Thermoelasticity of silicate perovskite and magnesiowustite and stratification of the earth's mantle. *Science, 257*, 1099–1101, 1992.

Troullier, N., and J. L. Martins, Efficient pseudopotentials for plane-wave calculations. *Physical Review B, 43*, 1993–2003, 1991.

Vanderbilt, D., Soft self-consistent pseudopotentials in a generalized eigenvalue formalism. *Physical Review B, 41*, 7892–7895, 1990.

Vinnik, L., B. Romanowicz, Y. LeStunff, and L. Makeyeva, Seismic anisotropy in the d'' layer. *Geophysical Research Letters, 22*, 1657–1660, 1995.

Wang, Y. B., D. J. Weidner, R. C. Liebermann, and Y. S. Zhao, P-V-T equation of state of $(Mg,Fe)SiO_3$ perovskite - constraints on composition of the lower mantle. *Physics of the Earth and Planetary Interiors, 83*, 13–40, 1994.

Watt, J. P., G. F. Davies, and R. J. O'Connell, The elastic properties of composite materials. *Reviews of Geophysics and Space Physics, 14*, 541–563, 1976.

Weidner, D. J., J. D. Bass, A. E. Ringwood, and W. Sinclair, The single-crystal elastic moduli of stishovite. *Journal of Geophysical Research, 87*, 4740–4746, 1982.

Wentzcovitch, R. M., Invariant molecular dynamics approach to structural phase transitions. *Physical Review B, 44*, 2358–2361, 1991.

Wentzcovitch, R. M., and L. Stixrude, Crystal chemistry of forsterite: a first principles study. *American Mineralogist, 82*, 663–671, 1997.

Wentzcovitch, R. M., J. L. Martins, and G. D. Price, *Ab initio* molecular dynamics with variable cell shape: application to $MgSiO_3$ perovskite. *Physical Review Letters, 70*, 3947–3950, 1993.

Wentzcovitch, R. M., N. L. Ross, and G. D. Price, Ab initio study of $MgSiO_3$ and $CaSiO_3$ perovskites at lower-mantle pressures. *Physics of the Earth and Planetary Interiors, 90*, 101–112, 1995.

Yeganeh-Haeri, A., Synthesis and re-investigation of the elastic properties of single-crystal magnesium silica perovskite. *Physics of the Earth and Planetary Interiors, 87*, 111–121, 1994.

Zaug, J. M., E. H. Abramson, J. M. Brown, and L. J. Slutsky, Sound velocities in olivine at earth mantle pressures. *Science, 260*, 1487–1489, 1993.

L. Stixrude, Department of Geological Sciences, 425 E. University Av., University of Michigan, Ann Arbor, MI 48109-1063